

RESEARCH ARTICLE

Combined Effects of Flow Diverting Strategies and Parent Artery Curvature on Aneurysmal Hemodynamics: A CFD Study

Jinyu Xu¹✉, Zhichen Wu²✉, Ying Yu¹, Nan Lv¹, Shengzhang Wang³, Christof Karmonik⁴, Jian-Min Liu^{1*}, Qinghai Huang^{1*}

1 Department of Neurosurgery, Changhai Hospital, Second Military Medical University, Shanghai, China, **2** School of International Relations and Public Affairs, Fudan University, Shanghai, China, **3** Department of Mechanics and Engineering Science, Fudan University, Shanghai, China, **4** Cerebrovascular Center, Department of Neurosurgery, Houston Methodist Hospital, Houston, TX, United States of America

✉ These authors contributed equally to this work.

* chstroke@163.com (JL); ocinhqh@163.com (QH)



OPEN ACCESS

Citation: Xu J, Wu Z, Yu Y, Lv N, Wang S, Karmonik C, et al. (2015) Combined Effects of Flow Diverting Strategies and Parent Artery Curvature on Aneurysmal Hemodynamics: A CFD Study. PLoS ONE 10(9): e0138648. doi:10.1371/journal.pone.0138648

Editor: Josué Sznitman, Technion - Israel Institute of Technology, ISRAEL

Received: June 24, 2014

Accepted: September 2, 2015

Published: September 23, 2015

Copyright: © 2015 Xu et al. This is an open access article distributed under the terms of the [Creative Commons Attribution License](https://creativecommons.org/licenses/by/4.0/), which permits unrestricted use, distribution, and reproduction in any medium, provided the original author and source are credited.

Data Availability Statement: All relevant data are within the paper and its Supporting Information files.

Funding: This research was supported by National Natural Science Foundation of China (Grant No. 81171092 and Grant No. 81171093), Rising-Star Program of Shanghai Science and Technology Committee (Grant no. 11QA1408400), National Key Technology R&D Program of the Ministry of Science and Technology of China (No. 2011BAI08B06 and No. 2011BAI08B14), and State Scholarship Fund of China Scholarship Council (No. 201406580004).

Abstract

Purpose

Flow diverters (FD) are increasingly being considered for treating large or giant wide-neck aneurysms. Clinical outcome is highly variable and depends on the type of aneurysm, the flow diverting device and treatment strategies. The objective of this study was to analyze the effect of different flow diverting strategies together with parent artery curvature variations on altering intra-aneurysmal hemodynamics.

Methods

Four ideal intracranial aneurysm models with different parent artery curvature were constructed. Computational fluid dynamics (CFD) simulations of the hemodynamics before and after applying five types of flow diverting strategies (single FD, single FD with 5% and 10% packing density of coils, two FDs with 25% and 50% overlapping rate) were performed. Changes in pressure, wall shear stress (WSS), relative residence time (RRT), inflow velocity and inflow volume rate were calculated and compared.

Results

Each flow diverting strategy resulted in enhancement of RRT and reduction of normalized mean WSS, inflow volume rate and inflow velocity in various levels. Among them, 50% overlapped FD induced most effective hemodynamic changes in RRT and inflow volume rate. The mean pressure only slightly decreased after treatment. Regardless of the kind of implantation of FD, the mean pressure, inflow volume rate and inflow velocity increased and the RRT decreased as the curvature of the parent artery increased.

Competing Interests: The authors have declared that no competing interests exist.

Conclusions

Of all flow diverting strategies, overlapping FDs induced most favorable hemodynamic changes. Hemodynamics alterations post treatment were substantially influenced by parent artery curvature. Our results indicate the need of an individualized flow diverting strategy that is tailored for a specific aneurysm.

Introduction

Endovascular treatment for intracranial aneurysms (IAs) has been developed over the past decade as an alternative to surgery. Stent-alone treatment, as one of the endovascular technique, allows not only for protection of the parent artery from occlusion, but also diversion of the blood flow from the aneurysm [1–4]. In order to enhance the diverting effect, the flow diverter (FD) device that is stent-like but with much higher metal coverage, has emerged in recent years. Its effectiveness in treating aneurysms had been demonstrated in both animal and clinical studies [5,6], especially for wide-necked, large or fusiform aneurysms [7–9].

Although FD is being increasingly deployed to treat cerebral aneurysms, clinical outcomes are still highly variable. Besides complete aneurysm occlusions in most cases, longer-term patency and delayed aneurysm rupture have been reported [10–13]. The FD does not act by only mechanically excluding the aneurysm from blood flow but—depending on the induced hemodynamic changes—initiates a process of thrombosis formation and endothelial remodeling to eventually seal the aneurysm. Hence the prognosis of FD-treated aneurysms will be mainly affected by changes in hemodynamics. Many factors may influence aneurysmal hemodynamics, such as variation in aneurysms geometry and the properties of FD itself. Differences in wire density had been studied using idealized geometries by Seshadhri et al. [14] and the FD with the highest wire density was shown to induce the most significant hemodynamic change. However, it is still not fully understood whether the variations in clinical outcome are related to different morphologies of the parent artery in particular its curvature, or the variable types of the flow diverting device and the particular treatment strategy. This study we designed to address the following questions:

1. How should we use the flow diverters for treating aneurysms? Single FD, multiple FDs or FD combined with loose-packing coils?
2. Should we plan the FD treatment based on patient specific vessel geometry, such as different parent vessel curvatures?

Materials and Methods

The Institution Review Board of Changhai Hospital, affiliated to the Second Military Medical University, approved this retrospective study, and the requirement for informed consent was waived. In addition, we have not conducted research outside our country of residence.

Vascular Models

Four ideal intracranial aneurysm models with wide necks that were usually considered for flow diverting treatments were constructed using 3DMAX8.0 (Autodesk USA). The perpendicular height, neck diameter and aspect ratio of these aneurysm models were 5 mm, 5 mm and 1, respectively. The length and diameter of their parent vessel was 30 mm and 4 mm. The

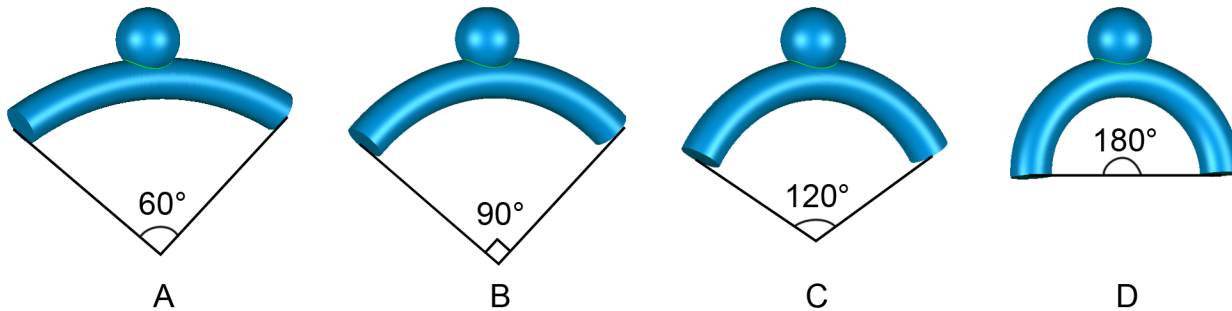


Fig 1. Four ideal intracranial aneurysm models with different parent vessels' curvature. A, 60°. B, 90°. C, 120°. D, 180°.

doi:10.1371/journal.pone.0138648.g001

curvatures of the parent vessel segments were 34.89, 52.33, 69.78, 104.67 m^{-1} , respectively (corresponding to the angles of the arc: 60°, 90°, 120° and 180°) (Fig 1).

From a retrospectively obtained pulsatile velocity waveform recorded with transcranial Doppler of a healthy subject, an average blood flow velocity waveform was calculated (flow spectrum envelope using Matlab 7.0 software, MathWorks, Natick, Massachusetts) (Fig 2). The maximum velocity magnitude was 1.49 m/s. Plug flow was used for the inlet and care was taken to ensure that the proximal section of the parent artery was longer than 10 artery diameters so that the flow profile could fully develop prior to the aneurysm ostium.

Virtual FD Treatment Models

Five different types of FD treatment strategies were simulated based on three common clinical practices: 1. single FD; 2. single FD assisted with coil embolization (5% packing density); 3. single FD assisted with coil embolization (10% packing density); 4. two overlapping FDs with 50% of overlapped rate at the aneurysm neck; and 5. two overlapping FDs with 25% of overlapped rate.

Virtual FD models were constructed (SolidWorks 2010, Dassault Systemes, Concord, Massachusetts) according to the design specifications of the FD (first-generation of the TUBRIDGE embolization device composed of 32 nickel–titanium alloy struts, including two parallel radio-opaque struts containing platinum (diameter = 0.05 mm), MicroPort Medical [Shanghai] Co. Ltd., China), which included the FD's inner/outer diameter, filament diameter, number of filaments and pitch as previously described [15]. The diameter of the FD was adjusted to match the diameter of the parent artery. The virtual FD models were bent (Abaqus 6.11, SIMULIA,

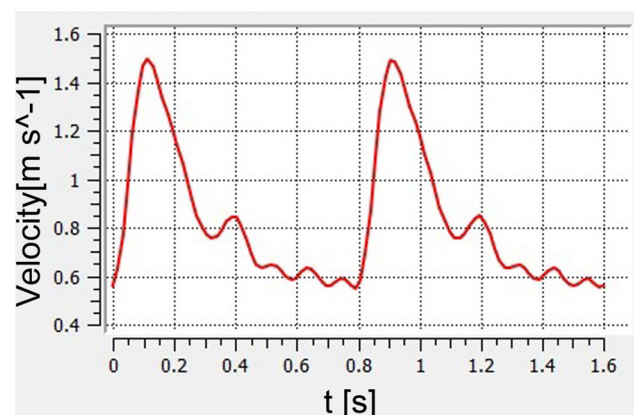


Fig 2. The flow velocity waveform based on transthoracic duplex Doppler examination.

doi:10.1371/journal.pone.0138648.g002

Table 1. Permeability of Each Aneurysm Models.

Aneurysm models	Volume of Aneurysm (cm ³)	Coil Diameter (mm)	Coil porosity	Coil permeability (m ² ×10 ⁻⁷)
60°	0.11536	0.25	0.95	6.89891
	0.11536	0.25	0.90	5.86593
90°	0.11487	0.25	0.95	6.89884
	0.11487	0.25	0.90	5.86588
120°	0.11472	0.25	0.95	6.89882
	0.11472	0.25	0.90	5.86586
180°	0.11335	0.25	0.95	6.89863
	0.11335	0.25	0.90	5.86570

doi:10.1371/journal.pone.0138648.t001

Providence, Rhode Island) to follow each parent vessels' curvature (uniquely defined by the angle of the ideal arc geometry) and stent struts not covering the ostium were removed GEOMAGIC STUDIO 9.0 (Geomagic USA). The metal coverage of each FD was 30%.

The endosaccular deployment of the platinum coils were modeled as porous medium as described by Mitsos et al. [16]. All coils had a diameter of 0.010 inch (i.e. 0.25 mm). The packing densities were chosen as 5% and 10%, which corresponds to a porosity of 0.95 and 0.90, respectively. Corresponding permeability was calculated from taking aneurysm volume and porosity into account (Table 1). The corresponding drag factor in the porous medium was estimated to $CD \approx 2.2$ [17].

CFD Meshing and Flow Modeling

The advantage of using ideal geometries allows the unique definition of the aneurysm ostium and the constant curvature provides an unambiguous approach of uniquely fitting the virtual FD models into the parent artery segment. The position of the implanted FD, of the porous medium representing the coils and of the two different overlapping FD configurations are shown in Fig 3. Each model was meshed (ICEM CFD 11.0, ANSYS, Canonsburg, PA) with the same reference mesh size to generate 1.01 to 1.72 million finite volume tetrahedral elements and wall prism elements (for accurate boundary layer resolution), with 2.03×10^3 to 3.51×10^3 elements per cubic millimeter [15]. Previous studies have shown that this mesh resolution is sufficient for hemodynamic simulations [18].

The governing equations underlying the CFD computation were the Navier-Stokes equations assuming laminar and incompressible flow. Blood was treated as a Newtonian fluid. Density and dynamic viscosity of blood were specified as $\rho = 1050 \text{ kg/m}^3$ and $\mu = 0.00345 \text{ Pa}\cdot\text{s}$, respectively. Vessel walls were assumed to be rigid with no-slip boundary conditions. On the inlet, the measured pulsatile velocity waveform obtained as described above was prescribed. The outlet was modeled as an open boundary with zero static reference pressure. The simulation was performed by CFX 11.0 (ANSYS, Canonsburg, PA). We discretized the whole cardiac cycle of 0.8 s by a time-step of 0.001 s. Three cardiac cycles were simulated to allow for the decay of initial transients, and results are reported from the last cycle only. The aneurysm geometries were isolated from their parent arteries for subsequent data analysis by a cut plane positioned at the ostium. We then post-processed and visualized the results of these simulations with CFX 11.0 (ANSYS, Canonsburg, PA).

Hemodynamic Parameters

Changes of the following hemodynamic parameters were calculated before and after the five types of flow diverting strategies: pressure, wall shear stress (WSS), relative residence time

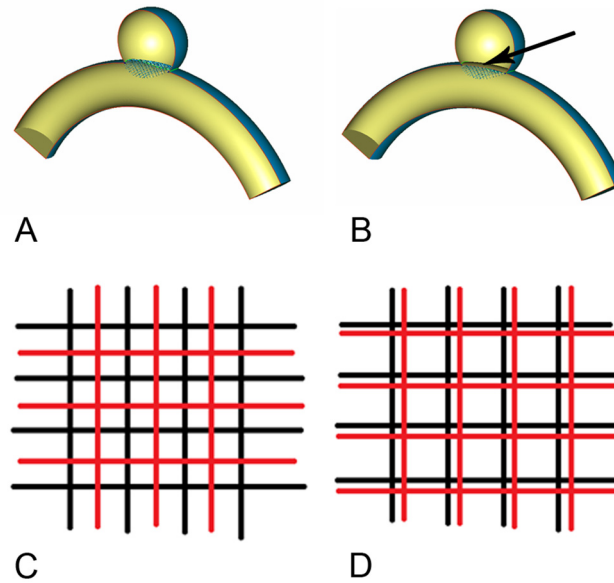


Fig 3. The geometry of models. A, the region of the FD model. B, the region of the FD and porous medium for coil, the interface (arrow) of the fluid (vessel region) and porous medium (aneurysm region). C, 50% overlapped rate of double FD models. D, 25% overlapped rate of double FD models.

doi:10.1371/journal.pone.0138648.g003

(RRT), inflow velocity and inflow volume rate. WSS (already time-averaged, as in Eq 1) was averaged over the sac area (the entire luminal surface of the aneurysm sac). In this study, the WSS distributions were normalized by the average parent vessel WSS in the same model to allow comparison among different models [19]. And as we assume that our models accurately reproduce 'healthy' or 'normal' WSS values in the parent vessel, the deviations from these values are best described by providing relative values (relative to these normal values). RRT, a combination of WSS and Oscillatory Shear Index (OSI), describes the slow flow adjacent to the aneurysm wall by providing a means of quantifying the residence time near the wall [20]. Thus, a metric termed RRT was defined to quantify the state of disturbed flow [21]:

$$WSS = \frac{1}{T} \int_0^T |wss_i| dt \tag{1}$$

$$OSI = \frac{1}{2} \left\{ 1 - \frac{\left| \int_0^T wss_i dt \right|}{\int_0^T |wss_i| dt} \right\} \tag{2}$$

$$RRT = \frac{1}{(1 - 2 \times OSI) \times WSS} = \frac{1}{\frac{1}{T} \int_0^T |wss_i| dt} \tag{3}$$

where wss_i is the instantaneous WSS vector and T is the duration of the cycle.

The mean inflow velocity and inflow volume rate were calculated at the aneurysm neck at peak systole ($t = 0.11s$). For this, the flow rate (separately for inflow and outflow) through the cut plane separating the aneurysm from the parent artery at the location of the ostium was

calculated as the product of the velocity component normal to the area and the area (built-in function available in CFX 11.0, ANSYS, Canonsburg, PA). We also visualized the inflow stream into the aneurysm sac on a plane oriented perpendicular to the aneurysm ostium before and after treatments.

Results

As the parent vessels' angle increases from 60°, 90°, 120° to 180°, the mean pressure and inflow volume rate increased and the RRT decreased (Fig 4). The mean pressure increased from 115.26, 136.49, 148.05 to 187.65 Pa, the inflow volume rate increased from 2.96, 3.73, 4.35 to 5.06 cm³/s, and the RRT decreased from 2.28, 1.84, 1.72 to 1.09. This tendency, however, was not obvious in the normalized mean WSS with the normalized mean WSS for 60° being smaller than the one for 180° (0.22 versus 0.26).

After single FD treatment, a similar trend in hemodynamic changes depending on parent artery curvature was observed. As the parent vessels' angle increased from 60°, 90°, 120° to 180°, the mean pressure grew from 111.72, 129.49, 143.88 to 175.99 Pa, the inflow volume rate also showed an upward trend from 0.58, 0.69, 0.85 to 1.33 cm³/s, and the RRT decreased from 14.09, 12.50, 9.15 to 4.39. Though the tendency of the normalized mean WSS was not as obvious as other hemodynamic parameters, the normalized mean WSS of 60° was still smaller than that of 180° (0.21 versus 0.25).

The influence of different FD treatment strategies on aneurysm hemodynamics was demonstrated in Fig 5. The mean pressure only slightly decreased after treatments, and no significant

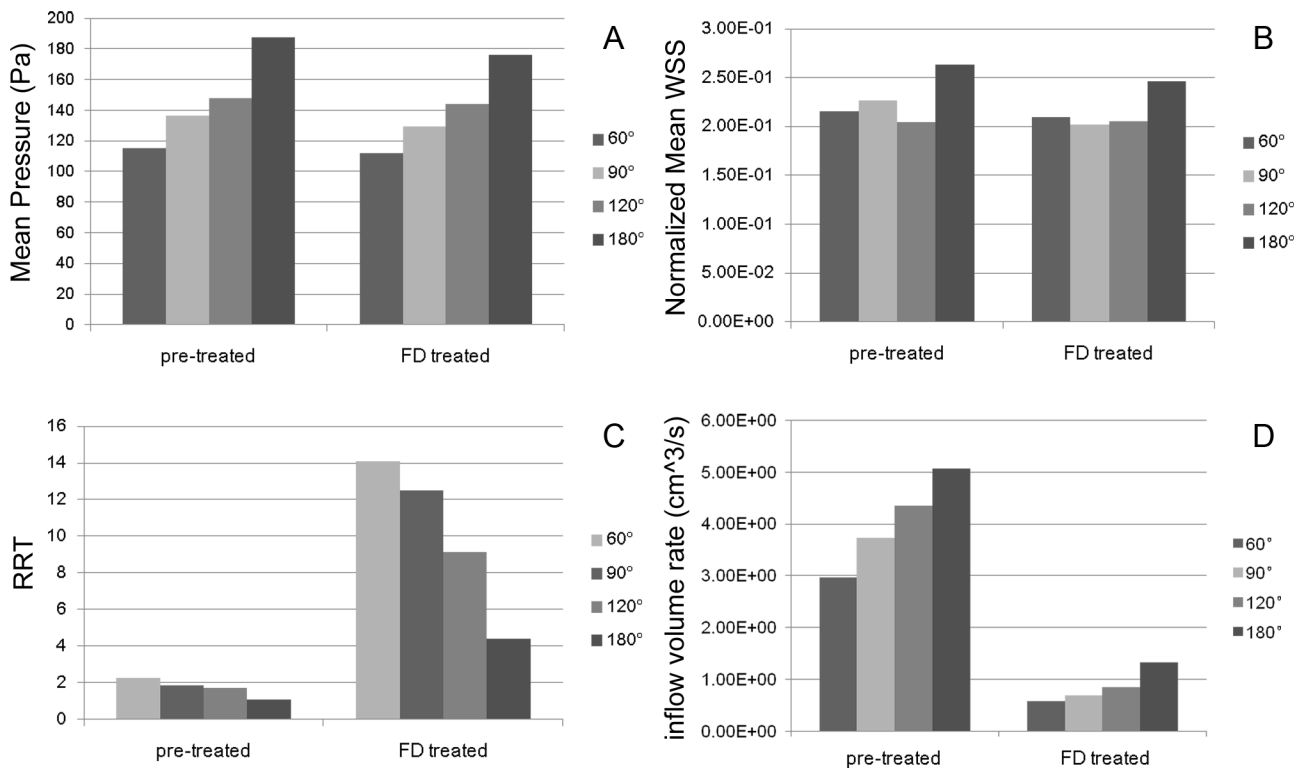


Fig 4. Quantitative hemodynamic results before and after FD treatment. Each panel shows the hemodynamic results for every parent vessels' curvature considered (first, second, third and fourth bars indicate 60°, 90°, 120° and 180° respectively). A, mean pressure. B, normalized mean WSS. C, RRT. D, inflow volume rate.

doi:10.1371/journal.pone.0138648.g004

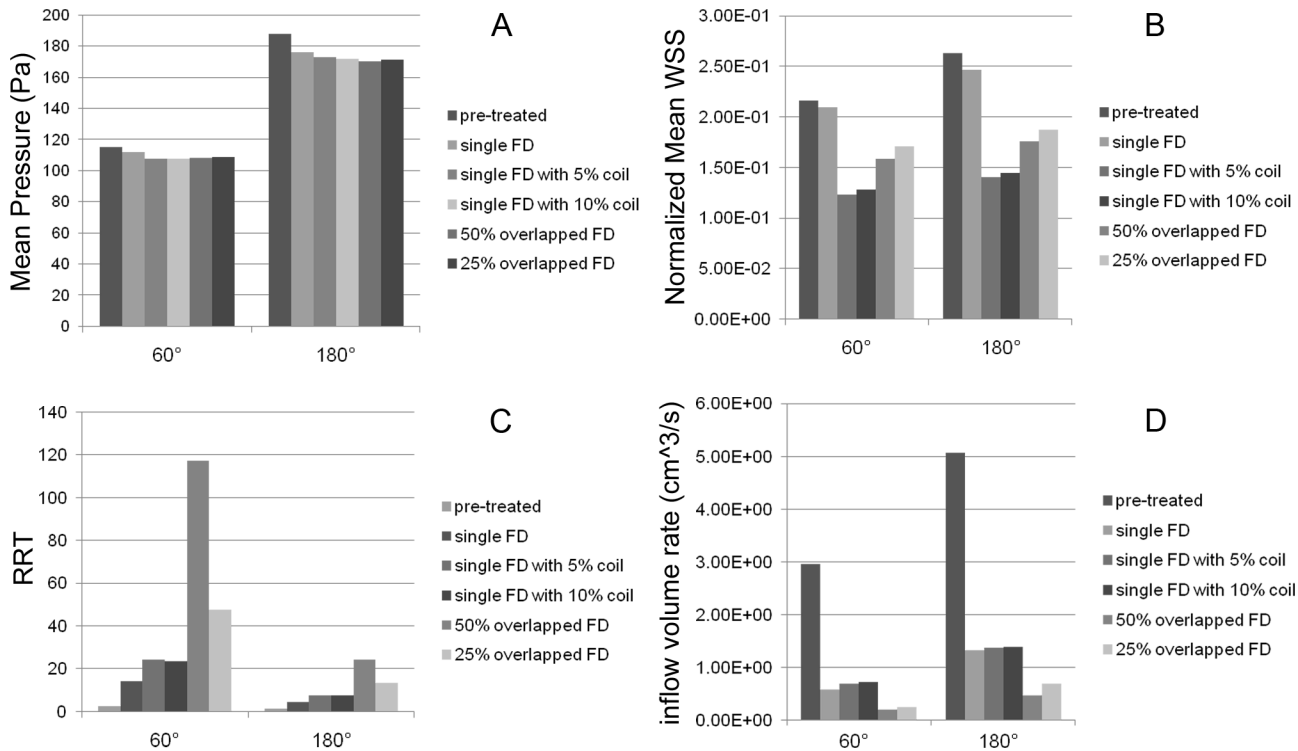


Fig 5. Quantitative hemodynamic results before and after each types of flow diverting methods. The two panels show the hemodynamic results for 60° and 180° parent vessels' curvature (first to sixth bars indicate pre-treated, single FD, single FD with 5% packing density coil, single FD with 10% packing density coil, overlapped FD with 50% overlapped rate and overlapped FD with 25% overlapped rate respectively). A, mean pressure. B, normalized mean WSS. C, RRT. D, inflow volume rate.

doi:10.1371/journal.pone.0138648.g005

differences were observed for the different FD treatment strategies. The RRT was enhanced, and the normalized mean WSS and inflow volume rate were reduced. Specifically, the reduction of normalized mean WSS was largest for the single FD combined with 5% coils, and smallest using only the single FD. The treatment using overlapped FD with 50% overlapped rate resulted in the most significant enhancement of RRT and reduction of inflow volume rate, while the single FD only showed the lowest enhancement of RRT. Combining single FD with 10% packing density coil showed the lowest reduction of inflow volume rate. There was no significant hemodynamic difference between the FD treatments combined with 5% and 10% packing density coil. There was also no significant difference in the change of normalized mean WSS and inflow volume rate between the two degrees of overlapping FDs, but significant differences were found for the increase of RRT.

The inflow velocity was substantially reduced after flow diverting treatment as shown (Fig 6) indicating that the FDs blocked and disrupted the inflow jets thereby reducing aneurysmal inflow. Among all five FD treatment strategies, the method of overlapping FD, in particular with a degree of 50% overlap, showed the most significant reduction in inflow velocity. The inflow jet into the aneurysm exhibited a consistent upward trend both before and after flow diverting treatments as the parent vessel curvature increased (Fig 6).

Discussion

In this study, we analyzed hemodynamic changes caused by different flow diverting treatment strategies together with varying degrees of parent artery curvature. All kinds of flow diverting

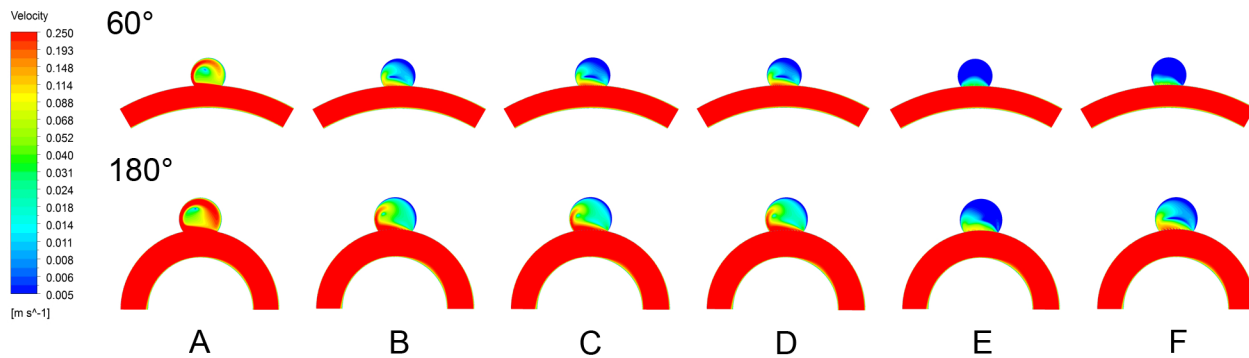


Fig 6. The velocity magnitudes of inflow stream of the aneurysm sac was plotted in logarithmic scale on the cut plane before and after each types of flow diverting methods for 60° and 180° parent vessels' curvature considered. A, pre-treated. B, single FD. C, single FD with 5% packing density coil. D, single FD with 10% packing density coil. E, overlapped FD with 50% overlapped rate. F, overlapped FD with 25% overlapped rate.

doi:10.1371/journal.pone.0138648.g006

strategies investigated resulted in enhancement of RRT and reduction of normalized mean WSS, inflow volume rate and inflow velocity. Except for the mean pressure, different types of flow diverting strategies led to different levels of hemodynamic changes. Moreover, the pressure, inflow velocity and inflow volume rate increased and the RRT decreased as the parent vessels' curvature increased, regardless of the way the FD was implanted.

Hemodynamic factors are commonly believed to play an important role in the pathogenesis, progression, and rupture of cerebral aneurysms. Specifically the hemodynamic-change-induced intra-aneurysmal thrombosis and thrombus are the most important processes after the endovascular treatment for healing, and the low-flow velocity relates to regions prone to thrombus formation [22]. These factors were supported by our previous study [23] that the higher RRT increment, more percentage of inflow volume reduction and location of stream inlet near the central part of the neck may be closely related to healing. It was also demonstrated that relative flow velocity and WSS reduction caused by FD implantation resulted in aneurysm thrombosis in a majority of cases [3]. Significant correlations between regions where CFD predicted either an increased flow residence time (RT) or low WSS and the regions where thrombus deposition was observed to occur using MRI in vivo has been previously demonstrated [24]. Reduction of blood flow into the aneurysm and of the flow velocity magnitude at the neck were found to be related to favorable outcome for FD treatment [4]. These results all imply the importance of hemodynamics for FD treatment outcome.

CFD studies using real patient geometries depend on many factors including parent artery curvature, aneurysm morphology. Using ideal geometries allows isolating the effect a single factor in this multifactorial space has on the overall hemodynamics. The boundary conditions we used are intended to represent the pressure drop across the artery segment containing the aneurysm. Inlet pressure is defined by the inlet velocity and outlet pressure is set to zero (as baseline) [3,4,10,18,23,25–30]. This approach of investigating the effects of the pressure gradient on a local artery segment is a commonly used and an accepted approach and therefore allows our results to be compared directly to simulations results reported in the literature obtained in this fashion [3,4,10,18,23,25–30].

Most previous studies were based on virtual stenting methods, including but not limited to the adaptive grid embedding technique, porous medium method, fast virtual stenting method [30–32]. Ma et al. [33] simulated the mechanical deployment of FDs in patient-specific aneurysms by using a finite element analysis (FEA) based workflow. Our previous study compared the real structural configurations of fully deployed FDs in vivo with those of virtual FDs, and demonstrated that both virtual and realistic FD deployment methods produced very similar

hemodynamic results, with metal coverage (MC) in-vivo being 24.97% (range 21.19 to 29.45%) and 30% for the simulations [15].

The hemodynamic efficiency of a stent or FD is related to several parameters, including strut shapes, porosity, quantity of stents, mesh hole shapes, metal coverage (MC) [34–36]. Liou et al. previously reported that the total inflow to the aneurysm is reduced to approximately 75%, 37.5% and 25% for the one-, two- and three-layer stented models, respectively, in comparison to an unstented model [37]. These findings are in agreement with our results when using two different degrees of FD overlap. Increase in RRT and reduction of normalized mean WSS, inflow volume rate and inflow velocity, were much more significant in the case with overlapping FDs than with single FD suggesting that the method of overlapping FDs, especially with a degree of 50%, tend to generate more favorable hemodynamic changes: Inflow at highest curvature (180 degrees) is reduced to a third compared to using a single FD, which is about the same factor as for the lowest curvature (60 degrees). At the same time, the total inflow at the highest curvature is still a factor 2.3 higher with 50% overlap than at the lowest curvature. These findings indicate the use of more than one FD is advisable only at high curvatures (> 60 degrees); at lower curvatures, risks for potential technical complications during the procedure and increased risk for thrombus formation in the parent artery may not outweigh the benefits of the achieved inflow reduction. Keeping these potential complications in mind, our results suggest that a higher and constant pore density over the entire length of the aneurysm neck leads indeed to a more efficient flow diversion and durable aneurysm occlusion [38]. Higher pore density can be achieved by more metal coverage. More struts may mean less flexibility of the final construct making a good fit into a tortuous curved arteries challenging. A new generation Tubridge FD device is being designed increasing the number of struts from 32 to 64 with the same material property for better pore density. We limited our new Tubridge FD to a maximum of 64 struts after carefully testing its flexibility and evaluating the probability of blocking or modifying the blood supply of small branches in recent clinical applications [39]. Covered stents are not used in the cerebral vasculature as they might block off small side branches and perforators causing stroke. The generality of our findings may be transferrable to other kinds of flow diverter devices with different size, shape, number of struts as inflow into the aneurysm pre and post FD treatment is mainly governed by the geometry of the parent vessel.

Hemodynamic changes can be affected not only by the FD deployment but also by the morphology of the aneurysm and the parent artery, as the morphologies of the parent artery and of the aneurysm are as important as hemodynamics in discriminating aneurysm rupture status [40,41]. Cebal et al. [42] showed that hemodynamics with a given geometry did not vary significantly with physiological variations of flow rate, blood pressure, and waveform. It can be inferred that intra-aneurysmal hemodynamics might be predominantly dependent on the geometry of the aneurysmal sac and its parent vessel [41,43,44]. Szikora et al. [45] noted that the aneurysm-to-parent-vessel angle was the most significant determinant of flow patterns in the sac. Our results also show a strong dependence of aneurysm hemodynamic on the curvature of the parent artery. Specifically, pressure, inflow volume rate and inflow velocity increased and the RRT decreased as the curvature increased.

Limitations

1. Although CFD allows simulating the intra-aneurysmal hemodynamic environment with potential validation by clinical data, it has inherent limitations. The biological process of aneurysm prognosis, which is also related to the function of platelets, the local thrombosis, aneurysm occlusion, is not been taken into account in the kind of CFD simulation performed here.

2. While modeling coils as porous media is easy to implement, it cannot account for the actual coil locations and for local differences in permeability (as employed here).
3. Due to the lack of vessel wall thickness and elasticity parameters for intracranial aneurysm, vessel walls were assumed rigid for this study. A more realistic approach may employ deformable vessel walls or fluid-solid coupling and should be used once accurate material properties for the aneurysm wall become available.
4. To make the simulations more realistic, patient-specific inflow and outflow boundary conditions should be based on measured values [46,47].
5. Finally, in order to compare the hemodynamic differences among aneurysm models with different vascular morphology, our study adopted ideal intracranial aneurysm models which only changed its parent vessels' curvature within 2D plane, not considering the influence of its parent vessels' 3D torsion.

Conclusion

In this study, we analyzed hemodynamic changes induced by different flow diverting strategies together with variation in the curvature of the parent artery. FDs overlapping by 50%, induced most favorable hemodynamic changes. Intra-aneurysmal flow was substantially influenced by the curvature of the parent artery indicating the need for an individualized flow diverting treatment strategy, such as the number of FD needed (perhaps by 'stacking' the FD or by using two overlapping devices) or the inclusion of coils with specific packing density, for a particular aneurysm.

Supporting Information

S1 Table. Quantitative hemodynamic results before and after each types of flow diverting methods for each vessels' curvature.

(PDF)

Acknowledgments

We gratefully acknowledge the Shanghai Supercomputer Center for so helpfully providing the mathematical software. We also gratefully thank MicroPort Medical (Shanghai) Co. Ltd. for providing the free flow-diverting stents.

Author Contributions

Conceived and designed the experiments: JX ZW QH JL. Performed the experiments: JX ZW YY. Analyzed the data: JX ZW NL. Contributed reagents/materials/analysis tools: JX ZW SW JL. Wrote the paper: JX QH CK. Revised the manuscript: JX QH CK.

References

1. Zhao KJ, Zhang YW, Xu Y, Hong B, Huang QH, Zhao WY, et al. Reconstruction of Saccular and Dissected Intracranial Aneurysms Using Solitaire™ AB Stents. *PLoS ONE*. 2013; 8(2): e57253. doi: [10.1371/journal.pone.0057253](https://doi.org/10.1371/journal.pone.0057253) PMID: [23468947](https://pubmed.ncbi.nlm.nih.gov/23468947/)
2. Wang K, Huang Q, Hong B, Li Z, Fang X, Liu J. Correlation of aneurysm occlusion with actual metal coverage at neck after implantation of flow-diverting stent in rabbit models. *Neuroradiology*. 2012; 54:607–613. doi: [10.1007/s00234-011-0922-7](https://doi.org/10.1007/s00234-011-0922-7) PMID: [21874284](https://pubmed.ncbi.nlm.nih.gov/21874284/)

3. Kulcsár Z, Augsburger L, Reymond P, Pereira VM, Hirsch S, Mallik AS, et al. Flow diversion treatment: intra-aneurysmal blood flow velocity and WSS reduction are parameters to predict aneurysm thrombosis. *Acta Neurochir (Wien)*. 2012; 154:1827–1834.
4. Zhang Y, Chong W, Qian Y. Investigation of intracranial aneurysm hemodynamics following flow diverter stent treatment. *Med Eng Phys*. 2013; 35:608–615. doi: [10.1016/j.medengphy.2012.07.005](https://doi.org/10.1016/j.medengphy.2012.07.005) PMID: [22884174](https://pubmed.ncbi.nlm.nih.gov/22884174/)
5. Szikora I, Nelson PK, Berentei Z, Kulcsar Z, Marosfoi M, Berez A. The potential of flow modification in the treatment of intracranial aneurysms. *Interv Neuroradiol*. 2008; 14:77–80. PMID: [20557779](https://pubmed.ncbi.nlm.nih.gov/20557779/)
6. Kallmes DF, Ding YH, Dai D, Kadirvel R, Lewis DA, Cloft HJ. A new endoluminal, flow-disrupting device for treatment of saccular aneurysms. *Stroke*. 2007; 38:2346–2352. PMID: [17615366](https://pubmed.ncbi.nlm.nih.gov/17615366/)
7. Nelson PK, Lylyk P, Szikora I, Wetzel SG, Wanke I, Fiorella D. The pipeline embolization device for the intracranial treatment of aneurysms trial. *AJNR Am J Neuroradiology*. 2011; 32: 34–40.
8. Byrne JV, Beltechi R, Yarnold JA, Birks J, Kamran M. Early experience in the treatment of intra-cranial aneurysms by endovascular flow diversion: a multicentre prospective study. *PLoS One*. 2010; 5:1–8.
9. Lylyk P, Miranda C, Ceratto R, Ferrario A, Scrivano E, Luna HR. Curative endovascular reconstruction of cerebral aneurysms with the pipeline embolization device: the Buenos Aires experience. *Neurosurgery*. 2009; 64:632–642. doi: [10.1227/01.NEU.0000339109.98070.65](https://doi.org/10.1227/01.NEU.0000339109.98070.65) PMID: [19349825](https://pubmed.ncbi.nlm.nih.gov/19349825/)
10. Cebal JR, Mut F, Raschi M, Scrivano E, Ceratto R, Lylyk P, et al. Aneurysm rupture following treatment with flow-diverting stents: computational hemodynamics analysis of treatment. *AJNR Am J Neuroradiol*. 2011; 32:27–33. doi: [10.3174/ajnr.A2398](https://doi.org/10.3174/ajnr.A2398) PMID: [21071533](https://pubmed.ncbi.nlm.nih.gov/21071533/)
11. Kulcsár Z, Houdart E, Bonafé A, Parker G, Millar J, Goddard AJ, et al. Intra-aneurysmal thrombosis as a possible cause of delayed aneurysm rupture after flow-diversion treatment. *AJNR Am J Neuroradiol*. 2011; 23:20–25.
12. van Rooij WJ, Sluzewski M. Perforator infarction after placement of a Pipeline flow-diverting stent for an unruptured A1 aneurysm. *AJNR Am J Neuroradiol*. 2010; 31:E43–44. doi: [10.3174/ajnr.A2034](https://doi.org/10.3174/ajnr.A2034) PMID: [20150311](https://pubmed.ncbi.nlm.nih.gov/20150311/)
13. Turowski B, Macht S, Kulcsár Z, Hänggi D, Stummer W. Early fatal hemorrhage after endovascular cerebral aneurysm treatment with a flow diverter (Silk-Stent): do we need to rethink our concepts? *Neuroradiology*. 2011; 53:37–41. doi: [10.1007/s00234-010-0676-7](https://doi.org/10.1007/s00234-010-0676-7) PMID: [20339842](https://pubmed.ncbi.nlm.nih.gov/20339842/)
14. Seshadhri S, Janiga G, Beuing O, Skalej M, Thévenin D. Impact of stents and flow diverters on hemodynamics in idealized aneurysm models. *J Biomech Eng*. 2011; 133:071005. doi: [10.1115/1.4004410](https://doi.org/10.1115/1.4004410) PMID: [21823744](https://pubmed.ncbi.nlm.nih.gov/21823744/)
15. Xu J, Deng B, Fang Y, Yu Y, Cheng J, Wang S, et al. Hemodynamic Changes Caused by Flow Diverters in Rabbit Aneurysm Models: Comparison of Virtual and Realistic FD Deployments Based on Micro-CT Reconstruction. *PLoS One*. 2013; 8(6):e66072. PMID: [23823503](https://pubmed.ncbi.nlm.nih.gov/23823503/)
16. Mitsos AP, Kakalis NM, Ventikos YP, Byrne JV. Haemodynamic simulation of aneurysm coiling in an anatomically accurate computational fluid dynamics model: technical note. *Neuroradiology*. 2008; 50:341–347. PMID: [18043912](https://pubmed.ncbi.nlm.nih.gov/18043912/)
17. Achenbach E. Influence of surface roughness on the cross-flow around a circular cylinder. *J Fluid Mech*. 1971; 46:321–335.
18. Wang S, Ding G, Zhang Y, Yang X. Computational haemodynamics in two idealised cerebral wide-necked aneurysms after stent placement. *Comput Methods Biomech Biomed Engin*. 2011; 14:927–937. doi: [10.1080/10255842.2010.502531](https://doi.org/10.1080/10255842.2010.502531) PMID: [22085241](https://pubmed.ncbi.nlm.nih.gov/22085241/)
19. Xiang JP, Natarajan SK, Tremmel M, Ma D, Mocco J, Hopkins LN, et al. Hemodynamic-Morphologic Discriminants for Intracranial Aneurysm Rupture. *Stroke*. 2011; 42:144–152. doi: [10.1161/STROKEAHA.110.592923](https://doi.org/10.1161/STROKEAHA.110.592923) PMID: [21106956](https://pubmed.ncbi.nlm.nih.gov/21106956/)
20. Himburg HA, Grzybowski DM, Hazel AL, LaMack JA, Li XM, Friedman MH. Spatial comparison between wall shear stress measures and porcine arterial endothelial permeability. *Am J Physiol Heart Circ Physiol*. 2004; 286: 1916–1922.
21. Lee SW, Antiga L, Steinman DA. Correlations among indicators of disturbed flow at the normal carotid bifurcation. *J Biomech Eng*. 2009; 131:061013. doi: [10.1115/1.3127252](https://doi.org/10.1115/1.3127252) PMID: [19449967](https://pubmed.ncbi.nlm.nih.gov/19449967/)
22. Rayz VL, Boussel L, Ge L, Leach JR, Martin AJ, Lawton MT, et al. Flow residence time and regions of intraluminal thrombus deposition in intracranial aneurysms. *Ann Biomed Eng*. 2010; 38:3058–3069. doi: [10.1007/s10439-010-0065-8](https://doi.org/10.1007/s10439-010-0065-8) PMID: [20499185](https://pubmed.ncbi.nlm.nih.gov/20499185/)
23. Huang Q, Xu J, Cheng J, Wang S, Wang K, Liu JM. Hemodynamic changes by flow diverters in rabbit aneurysm models: a computational fluid dynamic study based on micro-computed tomography reconstruction. *Stroke*. 2013; 44:1936–1941. doi: [10.1161/STROKEAHA.113.001202](https://doi.org/10.1161/STROKEAHA.113.001202) PMID: [23640830](https://pubmed.ncbi.nlm.nih.gov/23640830/)

24. Rayz VL, Boussel L, Lawton MT, Acevedo-Bolton G, Ge L, Young WL, et al. Numerical modeling of the flow in intracranial aneurysms: prediction of regions prone to thrombus formation. *Ann Biomed Eng.* 2008; 36:1793–1804. doi: [10.1007/s10439-008-9561-5](https://doi.org/10.1007/s10439-008-9561-5) PMID: [18787954](https://pubmed.ncbi.nlm.nih.gov/18787954/)
25. Lu G, Huang L, Zhang XL, Wang SZ, Hong Y, Hu Z, et al. Influence of hemodynamic factors on rupture of intracranial aneurysms: patient-specific 3D mirror aneurysms model computational fluid dynamics simulation. *AJNR Am J Neuroradiol.* 2011; 32:1255–1261. doi: [10.3174/ajnr.A2461](https://doi.org/10.3174/ajnr.A2461) PMID: [21757526](https://pubmed.ncbi.nlm.nih.gov/21757526/)
26. Naito T, Miyachi S, Matsubara N, Isoda H, Izumi T, Haraguchi K, et al. Magnetic resonance fluid dynamics for intracranial aneurysms—comparison with computed fluid dynamics. *Acta Neurochir (Wien).* 2012; 154:993–1001.
27. Qian Y, Takao H, Umezumi M, Murayama Y. Risk Analysis of Unruptured Aneurysms Using Computational Fluid Dynamics Technology: Preliminary Results. *AJNR Am J Neuroradiol.* 2011; 32:1948–1955. doi: [10.3174/ajnr.A2655](https://doi.org/10.3174/ajnr.A2655) PMID: [21903914](https://pubmed.ncbi.nlm.nih.gov/21903914/)
28. Bowker TJ, Watton PN, Summers PE, Byrne JV, Ventikos Y. Rest versus Exercise Hemodynamics for Middle Cerebral Artery Aneurysms: A Computational Study. *AJNR Am J Neuroradiol.* 2010; 31:317–23. doi: [10.3174/ajnr.A1797](https://doi.org/10.3174/ajnr.A1797) PMID: [19959776](https://pubmed.ncbi.nlm.nih.gov/19959776/)
29. Balossino R, Gervaso F, Migliavacca F, Dubini G. Effects of different stent designs on local hemodynamics in stented arteries. *J Biomech.* 2008; 41:1053–1061. doi: [10.1016/j.jbiomech.2007.12.005](https://doi.org/10.1016/j.jbiomech.2007.12.005) PMID: [18215394](https://pubmed.ncbi.nlm.nih.gov/18215394/)
30. Larrabide I, Kim M, Augsburg L, Villa-Urriol MC, Rufenacht D, Frangi AF. Fast virtual deployment of self-expandable stents: method and in vitro evaluation for intracranial aneurysmal stenting. *Med Image Anal.* 2012; 16:721–730. doi: [10.1016/j.media.2010.04.009](https://doi.org/10.1016/j.media.2010.04.009) PMID: [20627664](https://pubmed.ncbi.nlm.nih.gov/20627664/)
31. Appanaboyina S, Mut F, Löhner R, Putman CM, Cebal JR. Computational fluid dynamics of stented intracranial aneurysms using adaptive embedded unstructured grids. *Int J Numer Methods Fluids.* 2007; 57:475–493.
32. Augsburg L, Reymond P, Rufenacht DA, Stergiopoulos N. Intracranial stents being modeled as a porous medium: flow simulation in stented cerebral aneurysms. *Ann Biomed Eng.* 2010; 39:850–863. doi: [10.1007/s10439-010-0200-6](https://doi.org/10.1007/s10439-010-0200-6) PMID: [21042856](https://pubmed.ncbi.nlm.nih.gov/21042856/)
33. Ma D, Dargush GF, Natarajan SK, Levy EI, Siddiqui AH, Meng H. Computer modeling of deployment and mechanical expansion of neurovascular flow diverter in patient-specific intracranial aneurysms. *J Biomech.* 2012; 45:2256–2263. doi: [10.1016/j.jbiomech.2012.06.013](https://doi.org/10.1016/j.jbiomech.2012.06.013) PMID: [22818662](https://pubmed.ncbi.nlm.nih.gov/22818662/)
34. Lieber BB, Stancampiano AP, Wakhloo AK. Alteration of hemodynamics in aneurysm models by stenting: influence of stent porosity. *Ann Biomed Eng.* 1997; 25:460–469. PMID: [9146801](https://pubmed.ncbi.nlm.nih.gov/9146801/)
35. Kim YH, Xu X, Lee JS. The effect of stent porosity and strut shape on saccular aneurysm and its numerical analysis with lattice Boltzmann method. *Ann Biomed Eng.* 2010; 38:2274–2292. doi: [10.1007/s10439-010-9994-5](https://doi.org/10.1007/s10439-010-9994-5) PMID: [20300847](https://pubmed.ncbi.nlm.nih.gov/20300847/)
36. Lieber BB, Sadasivan C. Endoluminal scaffolds for vascular reconstruction and exclusion of aneurysms from the cerebral circulation. *Stroke.* 2010; 41:21–25.
37. Liou TM, Li YC. Effects of stent porosity on hemodynamics in a sidewall aneurysm model. *J Biomech.* 2008; 41:1174–1183. doi: [10.1016/j.jbiomech.2008.01.025](https://doi.org/10.1016/j.jbiomech.2008.01.025) PMID: [18377914](https://pubmed.ncbi.nlm.nih.gov/18377914/)
38. Sadasivan C, Cesar L, Seong J, Rakian A, Hao Q, Tio FO, et al. An original flow diversion device for the treatment of intracranial aneurysms: evaluation in the rabbit elastase-induced model. *Stroke.* 2009; 40:952–958. doi: [10.1161/STROKEAHA.108.533760](https://doi.org/10.1161/STROKEAHA.108.533760) PMID: [19150864](https://pubmed.ncbi.nlm.nih.gov/19150864/)
39. Zhou Y, Yang PF, Fang YB, Xu Y, Hong B, Zhao WY, et al. (2014) A Novel Flow-Diverting Device (Tubridge) for the Treatment of 28 Large or Giant Intracranial Aneurysms: A Single-Center Experience. *AJNR Am J Neuroradiol.* 2014; 35:2326–2333. doi: [10.3174/ajnr.A3925](https://doi.org/10.3174/ajnr.A3925) PMID: [24722307](https://pubmed.ncbi.nlm.nih.gov/24722307/)
40. Xu J, Yu Y, Wu X, Wu Y, Jiang C, Wang S, et al. Morphological and Hemodynamic Analysis of Mirror Posterior Communicating Artery Aneurysms. *PLoS ONE.* 2013; 8(1):e55413. doi: [10.1371/journal.pone.0055413](https://doi.org/10.1371/journal.pone.0055413) PMID: [23383184](https://pubmed.ncbi.nlm.nih.gov/23383184/)
41. Hoi Y, Meng H, Woodward SH, Bendok BR, Hanel RA, Guterman LR, et al. Effects of arterial geometry on aneurysm growth: three-dimensional computational fluid dynamics study. *J Neurosurg.* 2004; 101:676–681. PMID: [15481725](https://pubmed.ncbi.nlm.nih.gov/15481725/)
42. Cebal JR, Castro MA, Appanaboyina S, Putman CM, Millan D, Frangi AF. Efficient pipeline for image-based patient-specific analysis of cerebral aneurysm hemodynamics: Technique and sensitivity. *IEEE Trans Med Imaging.* 2005; 24:457–467. PMID: [15822804](https://pubmed.ncbi.nlm.nih.gov/15822804/)
43. Hassan T, Timofeev EV, Saito T, Shimizu H, Ezura M, Matsumoto Y, et al. A proposed parent vessel geometry-based categorization of saccular intracranial aneurysms: Computational flow dynamics analysis of the risk factors for lesion rupture. *J Neurosurg.* 2005; 103:662–680. PMID: [16266049](https://pubmed.ncbi.nlm.nih.gov/16266049/)

44. Ujiie H, Tachibana H, Hiramatsu O, Hazel AL, Matsumoto T, Ogasawara Y, et al. Effects of size and shape (aspect ratio) on the hemodynamics of saccular aneurysms: A possible index for surgical treatment of intracranial aneurysms. *Neurosurgery*. 1999; 45:119–130. PMID: [10414574](#)
45. Szikora I, Paal G, Ugron A, Nasztanovics F, Marosfoi M, Berentei Z, et al. Impact of aneurysmal geometry on intraaneurysmal flow: a computerized flow simulation study. *Neuroradiology*. 2008; 50:411–421. doi: [10.1007/s00234-007-0350-x](#) PMID: [18180916](#)
46. Karmonik C. Toward improving fidelity of computational fluid dynamics simulations: boundary conditions matter. *AJNR Am J Neuroradiol*. 2014; 35:1549–1550. doi: [10.3174/ajnr.A3984](#) PMID: [24763411](#)
47. Moon JY, Suh DC, Lee YS, Kim YW, Lee JS. Considerations of blood properties, outlet boundary conditions and energy loss approaches in computational fluid dynamics modeling. *Neurointervention*. 2014; 9:1–8. doi: [10.5469/neuroint.2014.9.1.1](#) PMID: [24642855](#)